Applied Thermal Engineering 188 (2021) 116628

Contents lists available at ScienceDirect

Applied Thermal Engineering

journal homepage: www.elsevier.com/locate/apthermeng

# Numerical investigation of swirl effects on a short natural draft dry cooling tower under windless and crosswind conditions

Yuchen Dai [a,*], Yuanshen Lu [a], Alexander Y. Klimenko [a], Ying Wang [b], Kamel Hooman [a]

[a] School of Mechanical and Mining Engineering, The University of Queensland, Brisbane, Australia
[b] School of Energy and Power Engineering, University of Shanghai for Science and Technology, Shanghai, China

ARTICLE INFO

*Keywords:*
Swirl
Buoyancy
Plume
Crosswind
Natural draft dry cooling towers

ABSTRACT

Swirling motions have been proven to improve the thermal performance of short natural draft dry cooling towers by reducing the cold air inflow and increasing the draft speed. However, crosswind influences on the favourable swirl effects have not been investigated. To fill this gap, 3-Dimensional simulations of a short natural draft dry cooling tower are carried out. Three different locations of the swirl generator, with solid body rotation, are compared under windless and crosswind conditions. The results show that, with no wind present, introducing swirling motions right above the heat exchangers is found to be the optimal location for improving around 40% of the reduced thermal performance, which is casued by cold air inflow penetration. On the other hand, as the swirl intensity further increases after the cold air inflow is eliminated, locating it at the tower outlet performs the best on the air draft speed enhancement, and thus further increases approximately 17% of the heat transfer rate at the angular frequency input of 2 $s^{-1}$. In the presence of crosswind and windbreak walls, air flows through the heat exchangers and tower non-uniformly. By mounting the swirl generator right above the heat exchangers, the uniform index of the heat flux can be improved by 5% with 1 $s^{-1}$ angular frequency input. More importantly, inducing swirls at the tower outlet is still the optimal choice for increasing the air draft speed through the tower. With 2 $s^{-1}$ angular frequency input, the thermal performance of the tower can be enhanced by 11~17% in accordance with the crosswind speed.

## 1. Introduction

Small scale power generation systems, i.e. in the sub-10 MWe range, are vital to mining sites and remote communities in Australia [1]. As a result, all the components including cooling towers need to be scaled down. Under such conditions, a 20-m-height natural draft dry cooling tower (NDDCT) has been designed and built in the Gatton campus at the University of Queensland. Experimental measurements have illustrated two major differences between short NDDCTs and the tall (over 100 m) counterparts: cold air inflow under windless conditions, and the tower response to crosswind [2,3]. For buoyant duct flows with extremely low Froude number *Fr*, i.e. low flow speed with high fluid temperature difference, a contraction effect on the plume occurs right after the hot flow leaves the duct. This is also known as the plume neck, as fundamentally explained by Hunt and Kaye [4]. For short NDDCTs or those with high flow resistance in the tower with extremely low *Fr* value, a plume neck forms above the tower near the cross-section circular edge, in the vicinity of which the cold ambient air mixes with the hot plume while the axial velocity is quite low due to the boundary layer effect. Thus, the mixed air is not entrained by the plume, but instead penetrates into the tower. This phenomenon has been observed in our full-scale tower experiments conducted under windless conditions and led to a non-negligible deteriorating effect on the thermal performance of the tower [3]. Subsequent studies have reported the transient characteristics of the cold air inflow penetration and its reduction by introducing swirling motions inside the tower [5,6].

For large scale NDDCTs, continuously declining trends on the thermal performance are generally observed with the increment of crosswind speeds, as reported in [7,8]. To mitigate the deteriorating wind effects, windbreak walls or deflectors are mainly adopted since they have been proven to be the most effective way for engineering purposes [3]. By carrying out both experimental and numerical investigations on a 160-m-height NDDCT, du Preez and Kröger [9] concluded that the optimal height of the walls is approximately one third of the inlet height of the tower. Zhai and Fu [10] numerically investigated windbreak walls with different widths for two 125-m-tall NDDCTs. The results indicated that, placing the walls at lateral sides of towers recovers the cooling

* Corresponding author.
*E-mail address:* yuchen.dai@uq.edu.au (Y. Dai).

https://doi.org/10.1016/j.applthermaleng.2021.116628
Received 7 September 2020; Received in revised form 3 January 2021; Accepted 20 January 2021
Available online 10 February 2021
1359-4311/

**Nomenclature**

| | |
|---|---|
| $\Delta n$ | thickness of the porous zone, m |
| $A$ | area, $m^2$ |
| $c_p$ | specific heat capacity, J/(kg·K) |
| $f$ | key variables |
| $Fr$ | Froude number |
| $Fs$ | safty factor |
| $g$ | acceleration of gravity, $m/s^2$ |
| $G_b$ | turbulent kinetic energy due to buoyancy, $m^2/s^2$ |
| $G_k$ | turbulent kinetic energy due to mean velocity gradient, $m^2/s^2$ |
| $H$ | clearance height of the tower, m |
| $h$ | heat transfer coefficient, $W/(m^2{\cdot}K)$ |
| $K$ | resistance coefficient |
| $k$ | turbulent kinetic energy, $m^2/s^2$ |
| $N$ | order of accuracy |
| $Nu$ | Nusselt number |
| $p$ | pressure, Pa |
| $Pr$ | Prandtl number |
| $Q$ | heat transfer rate, W |
| $q$ | heat flux, $W/m^2$ |
| $r$ | radius, m |
| $Rc$ | convergence ratio |
| $Re$ | Reynolds number |
| $Rf$ | refinement factor |
| $T$ | temperature, K |
| $t$ | time, s |
| $u$ | velocity, m/s |
| $z$ | elevation, m |
| $\beta$ | thermal expansion coefficient, 1/K |
| $\epsilon$ | turbulent dissipation rate, $m^2/s^3$ |
| $\gamma$ | uniformity index |
| $\Gamma_\phi$ | diffusion coefficient, kg/(m·s) |
| $\mu$ | dynamic viscosity, kg/(m·s) |
| $\omega$ | angular velocity, 1/s |
| $\phi$ | scalar variable |
| $\rho$ | density, $kg/m^3$ |
| $\sigma$ | turbulent Prandtl number |
| 0 | inlet |
| $\infty$ | ambient |
| ad | air downstream |
| a | air side |
| bl | bottom layer |
| cw | crosswind |
| e | effective |
| hx | heat exchangers |
| ref | reference |
| sf | superficial |
| t | turbulent |
| $r, \theta, z$ | radial, tangential, axial direction |

efficiency around 50%, and the optimal range of the width is from 10 to 20 m for the towers. Goodarzi and Keimanesh [11] numerically compared radiator-type windbreak walls with solid ones for a 103-m-height NDDCT, and pointed out the superiority of the former one, especially at the crosswind speed of 3 m/s. Chen et al. [12,13] proposed windbreak walls with 10 inside and 2 outside of a 170-m-tall NDDCT. The numerical results showed that the overall thermal performance of the cooling system can be improved by the combined configuration, though a slight decrement in the heat rejection rate of frontal sectors was observed. Wu et al. [14] adopted windbreak walls with arc curvature, or deflectors, outside the vertical heat exchangers of a 150-m-tall NDDCT by means of numerical simulations, pointing out that, with the crosswind speed of 20 m/s, a 50% enhancement on the total air mass flow rate can be achieved by doing so. Ma et al. [15] employed windbreak walls with different setting angles outside a 173-m-height NDDCT. Those authors numerically found that the optimized setting angle for each windbreak wall is the air inflow deviation angle of the corresponding cooling delta's inlet when the wind speed varies from 0 to 8 m/s; while it is exactly in the radial direction at crosswind speed larger than 10 m/s. By dividing each windbreak wall into 3 rotatable columns, their following study proposed a rotational concept of the walls to optimize the effect, and the results indicated that, at the wind speed of 8 m/s, the improvement on the thermos-flow performance can be further increased by around 2.5% in comparison with the radially arranged windbreak walls [16]. Additionally, they indicated that the cooling capacity of the tower can be enhanced by 15.6% to the maximum as the apex angle of the delta-type radiators increases from 48° to 60° [17].It is found that, whatever the heat exchangers are vertically or horizontally arranged, the main purpose of the windbreak walls is to guide the wind direction normal to the frontal surface of heat exchangers, and thus improving augmenting the heat transfer from the heat exchangers.

Different from the continuously decreasing trends on the thermal performance of large scale NDDCTs (over 100 m height) caused by crosswind as mentioned above, Lu [2] experimentally found that, as the crosswind speed increases, the thermal performance decreases first and then increases for a small scale NDDCT. This interesting behaviour was explained by the much lower air draft speed in short NDDCTs compared with that in large counterparts, so the forced convection caused by the crosswind, instead of the natural one by buoyancy, is more likely to dominate the heat transfer mechanism inside the tower. He also proposed tri-blade-like windbreak walls underneath the horizontally arranged heat exchangers to investigate how they influence the crosswind effects, and demonstrated that the adverse part of the crosswind influence on the thermal performance can even be turned into positive. In addition, the optimal angle of wind attack of the walls was found to be 0 ° under the crosswind ranged from 0 to 20 m/s.

To augment heat transfer in a cooling tower, swirl generation was proposed in [18], in the absence of crosswind, to enhance the air mass flow rate and thus increase the thermal performance. Eight air ejectors were embedded on the inner tower wall with specific angles to generate swirling momentum. The results indicate that, swirling motions significantly enhance the thermal performance of the tower by increasing the air draft speed. Interestingly, even by arranging the air ejectors to create only tangential momentums one can accelerate the axial velocity through the tower. A subsequent study by Dai et al. [19] fundamentally explained it from the area-weighted mean gauge pressure reduction at the tower outlet caused by tangential momentums. It was shown that while the mean gauge pressure difference between the tower outlet and the heat exchanger elevations remains the same, the radial pressure profiles are changed. Hence, the mean gauge pressure at the heat exchanger is consequently decreased, leading to an enhanced air draft. Those authors also pointed out that the enhancement is influenced by cold air inflow under windless condition and side effects by extremely strong swirl intensities, including vortices formed adjacent to the inner tower wall and vortex breakdown above the tower. However, the crosswind effect, which is prevailing for short towers, has not been investigated for a tower with induced swirl. In the absence of crosswind, a swirling buoyant flow from NDDCTs can be divided into confined swirl (vortical flow inside the tower) and free swirl (vortical flow above the tower). However, the free swirl can be highly affected in the presence of crosswind. Studies on the confined swirl, usually in tubes or pipes, were mainly concerned with the swirl decay [20–22], boundary layer influences [23,24] and vortex breakdown [25,26], while investigations of the free ones in the presence of crosswind can only be found in literature related to tornadoes and fire whirl as well as tilted vortex tubes [27,28].

The aforementioned literatures regarding swirl effects on the thermal performance of NDDCTs have not included how they perform in the presence of crosswind. Hence, this study is conducted to fill the gap, by means of numerical simulations. As part of the investigations on a small scale NDDCT (20 m height) with horizontally arranged heat exchangers, the tri-blade-like windbreak walls with the optimal angle of wind attack (0 °) [2] are adopted underneath the heat exchangers against the crosswind effects. With horizontal heat exchangers, it is advisable to induce swirl in the tower downstream the heat exchanger as otherwise the swirling motions can be destroyed as the air crosses the compact finned heat exchanger. With strong wind, the air is pushed inside the tower and interacts with the swirl-enhanced draft.

## 2. Numerical method

The $k$-$\epsilon$ realizable model can successfully predict flows involving swirl, boundary layers with strong adverse pressure gradients, separations, and recirculation, as indicated in [29]. It has also been proven to be appropriate for both crosswind effects on NDDCTs [7,30] and swirl [31] simulations.

### 2.1. Governing equations and solver

Air is modelled as an incompressible fluid with the Boussinesq's approximation to model the buoyancy term in the $z$-component of the momentum equation. Turbulence is modelled using the $k$-$\epsilon$ realizable model. The general form of the governing equations can be expressed as

$$\frac{\partial \rho \phi}{\partial t} + \nabla \cdot (\rho \vec{u} \phi - \Gamma_\phi \nabla \phi) = S_\phi \tag{1}$$

where the generalized scalar quantity $\phi$, diffusion coefficient $\Gamma_\phi$ and source term $S_\phi$ are defined in Table 1.

Simulations are performed using the commercially available CFD software package ANSYS 19.0. The SIMPLE algorithm is used for the pressure–velocity coupling. QUICK scheme is applied for the momentum, swirl velocity, turbulence kinetic energy, and turbulence dissipation rate with under-relaxation factors. Convergence criteria, the relative difference between the successive numerical value of the dependent variables, are set as $10^{-5}$, except for the axial velocity and continuity where $10^{-6}$ is set. Further, the transient solver is adopted to solve the conservation equations in a time-dependent manner, and then the steady-state solutions have been compared with the time-averaged transient counterparts, indicating that the difference is negligibly small. The governing equations are discretised by a second order implicit scheme for the spatial terms and transient formulation. The time step is determined as

$$\Delta t = \frac{CFL \Delta x}{u_{\mathrm{ref}}} \tag{2}$$

where the Courant-Fredrichs-Lewy number, $CFL$, is set to be 5 in accordance with [32]; the minimum mesh size $\Delta x$ is 0.0008 m; the reference velocity $u_{\mathrm{ref}}$ is 0.8 m/s [33]. Hence, the time step is prescribed as 0.005 s.

**Table 1**
Summary of governing equations.

| Equation | $\phi$ | $\Gamma_\phi$ | $S_\phi$ |
|---|---|---|---|
| Continuity | 1 | 0 | 0 |
| $x$-momentum | $U$ | $\mu_e$ | $-\frac{\partial p}{\partial x} + \nabla \cdot \left(\mu_e \frac{\partial}{\partial x} \vec{u}\right) + F_x$ |
| $y$-momentum | $V$ | $\mu_e$ | $-\frac{\partial p}{\partial y} + \nabla \cdot \left(\mu_e \frac{\partial}{\partial y} \vec{u}\right) + F_y$ |
| $z$-momentum | $W$ | $\mu_e$ | $-\frac{\partial p}{\partial z} + \nabla \cdot \left(\mu_e \frac{\partial}{\partial z} \vec{u}\right) + \rho_\infty g \beta (T - T_\infty) + F_z$ |
| Energy | $T$ | $\frac{K_e}{c_p}$ | $\frac{1}{c_p}\left(\frac{qA_c}{V_c}\right)$ |
| Turbulent energy | $k$ | $\frac{\mu_e}{\sigma_k}$ | $G_k + G_b - \rho\epsilon$ |
| Energy dissipation | $\epsilon$ | $\frac{\mu_e}{\sigma_\epsilon}$ | $C_{1\epsilon}\frac{\epsilon}{k}(G_k + C_{3\epsilon}G_b) - C_{2\epsilon}\rho\frac{\epsilon^2}{k}$ |

where $\mu_e = \mu + \mu_t; \mu_t = C_\mu \rho \frac{k^2}{\epsilon}; K_e = K + K_t; K_t = \frac{c_p \mu_t}{Pr_t}$

$G_k = \mu_t S^2; G_b = g\beta \frac{\mu_t}{Pr_t}\frac{\partial T}{\partial z}; \beta = \frac{1}{T_\infty}|_{p_\infty}$

$C_1 = \max\left[0.43, \frac{S\frac{k}{\epsilon}}{S\frac{k}{\epsilon} + 5}\right]; C_{1\epsilon} = 1.44; C_{2\epsilon} = 1.92; C_{3\epsilon} = \tanh\left(\frac{V}{U}\right)$

$\sigma_k = 1.0; \sigma_\epsilon = 1.44; Pr = 0.74; Pr_t = 0.85; T_\infty = 293.15$

### 2.2. Computational domain and boundary conditions

CFD simulations are conducted on a computational domain which is large enough to eliminate the edge effects, as shown in Fig. 1. The tower dimension corresponds to the size of the short NDDCT [3] while the shape remains cylindrical. The tri-blade-like windbreak walls with the optimal angle of wind attack 0° are introduced to guide the crosswind since they have been proven to improve the cooling performance of a short NDDCT with increased crosswind velocity [2]. Three swirl source zones with the same thickness (0.1 m) located inside the tower at different elevations are investigated. These elevations, as shown in Fig. 1, are right above the heat exchangers (zone 1); tower middle layer (zone 2); and tower outlet (zone 3).

Note that an unrealistic expansion effect might occur on the flow after it passes through the heat exchangers in CFD simulation, which is provoked by the radiator model with resistance coefficients [34]. Hence, a porous zone is adopted to simulate the heat exchangers resistance, and a radiator model with heat transfer coefficients and a constant temperature is applied on its top-surface, to avoid the numerical errors. The thickness of the porous zone is the same as that of the heat exchanger bundles in Gatton tower as 0.3 m. The inlet height is from ground to the up-surface of the porous zone. The porous model is achieved by adding momentum source terms of $i^{\mathrm{th}}$ ($x$, $y$ or $z$) direction to the standard fluid flow equations. The source term contains viscous and inertial losses as follow

$$S_i = -\left(C_1 \mu u_i + C_2 \frac{1}{2} \rho |u| u_i\right) \tag{3}$$

where the inverse of permeability $C_1$ and inertial resistance factor $C_2$ are both determined by the friction factor of heat exchangers and the porous zone thickness $\Delta n$ [3].

In the swirl source zones, the tangential velocity profile we prescribed is implemented by adding a source term in the tangential momentum equation. According to the UDF Manual in ANSYS FLUENT User's Guide [35], the added function should compute the source and return it to the solver. The solver linearizes source terms in order to enhance the stability and convergence of a solution. Hence, it is necessary to specify the dependent relationship between the source and solution variables, in the user defined function, in the form of derivative of the source term only depending on the solution variable. In this study, the solution variable is the tangential velocity profile, so the specified source term $\phi_\theta$ is expressed as

$$\frac{\partial \phi_\theta}{\partial u_\theta} = -C(u_\theta - u_{\theta 0}) \tag{4}$$

where $u_{\theta 0}$ is the specified tangential velocity; $C$ is the source coefficient with the unit of $kg/m^4$, which will result in the desired units of $N/m^3$ for

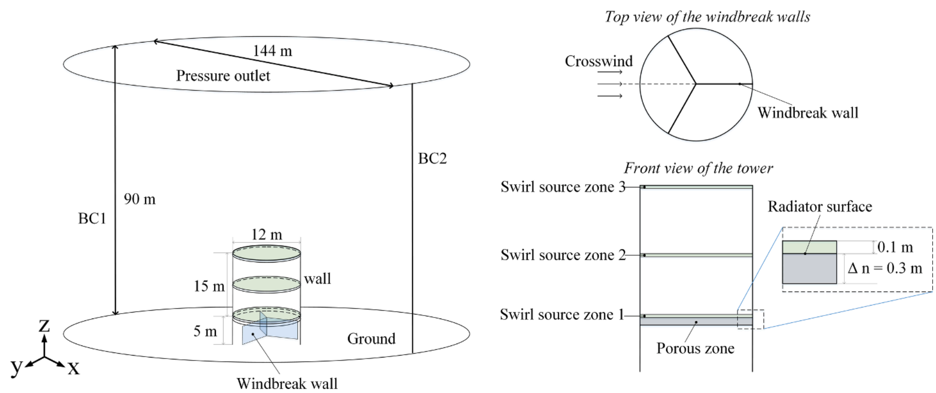


**Fig. 1.** Computational domain and tower dimensions.

the source $\phi_\theta$. Since the desired tangential velocity magnitude is 1 m/s, the source coefficient $C$ is set to be $10^5$ kg/m$^4$ so that the tangential velocity profile on the source zone up-surface can be guaranteed. An example of the desired tangential velocity profile (solid body rotation $u_{\theta 0} = r\omega$) compared to that on the source zone surface is shown in Fig. 2. As seen, the deviation is quite slight and thus can be neglected.

In addition, it has been pointed out that the standard wall function cannot predict complex flow including swirling flows due to the linear momentum exchange (based on Prandtl's mixing length assumption) [21]. Thus, the two-layer model is adopted to simulate the near wall region, which is implemented through the enhanced wall treatment with adequately fine mesh adjacent to the wall, i.e. $y^+ \approx 1$, in ANSYS FLUENT. The heat exchanger surface temperature and the ambient temperature are set to be 60 °C (333.15 $K$) and 20 °C (293.15 K), respectively. This further proves the validity of the Buossinesq approximation since $\beta \Delta T \approx 0.1 \ll 1$. Within the temperature difference range (40 °C) in this study, changes in the thermal conductivity, viscosity, and specific heat are negligible. Thus, the air properties are set to be constants as shown in Table 2.

The thermal boundary conditions for all the walls, including the ground and tower walls are adiabatic. Under windy conditions, the temperature of the velocity inlet boundary condition is set to be the same as the ambient one as 20 °C . The air side heat transfer coefficient correlations pertinent to the heat exchangers used in Gatton tower, can be derived from [3] as

$$h_a = 1.9648u_{sf}^2 + 9.9857u_{sf} + 2.3285 \quad (5)$$

Under windless conditions, the boundary conditions 1 and 2, pertinent to BC1 and BC2 in Fig. 1, are both set as pressure inlet, while in the presence of crosswind, BC1 and BC2 are set as velocity inlet and pressure outlet, respectively. The velocity profile is applied in BC1 as [3,2]

$$\frac{u_{cwp}}{u_{cw}} = \left(\frac{z}{z_{ref}}\right)^{0.2} \quad (6)$$

where the reference height, $z_{ref}$, is 5 m at which the crosswind speed was measured in the Gatton tower experiment [3].

At both inlet and outlet boundaries, the temperature and pressure are prescribed to be the same as ambient counterparts. Due to the low-turbulence level of advection natural wind at the computational domain boundaries, the impacts of the turbulence intensity as well as viscosity ratio are both negligible, as indicated in [36]. Regarding the Gatton tower simulation, it also has been proven that the turbulence is mainly caused by the boundary layer development and separation near the tower body, while the turbulence at the inlet and outlet boundaries of the domain has negligible influences [3,37]. Hence, 0.1% and 0.1 are fixed for turbulence intensity and viscosity ratio, respectively.

**Table 2**
Constant air properties used in the simulations.

| Air property | Value |
|---|---|
| Density (kg/m$^3$) | 1.204 |
| Specific heat (J/kg·K) | 1007 |
| Dynamic viscosity (kg/m·s) | $1.825 \times 10^{-5}$ |
| Thermal conductivity (W/m·K) | $2.514 \times 10^{-2}$ |
| Thermal expansion coefficient (1/K) | $3.411 \times 10^{-3}$ |

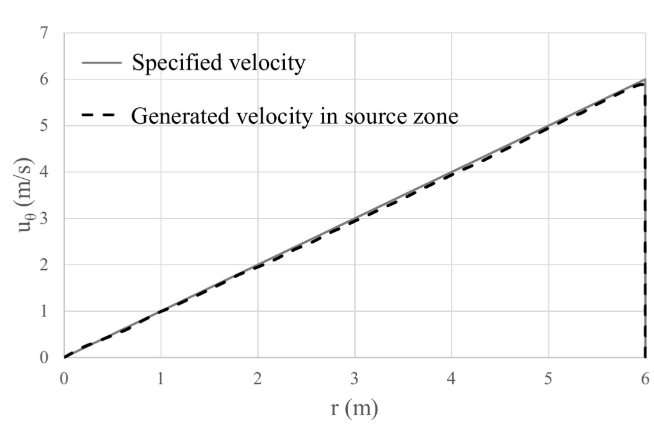


**Fig. 2.** Comparison between the desired velocity profile and the generated one in source zone ($\omega = 1$ s$^{-1}$).

### 2.3. Grid independence analysis

The Grid Convergence Index (GCI) [38] is employed for the grid independence analysis. Five sets of grids (coarse to fine) are selected with refinement factors higher than 1.3 (mainly performed inside the tower, with the grids adjacent to the outside of the tower), and the corresponding grid numbers are 0.58, 0.92, 1.46, 2.42, 3.67 million, respectively. Three key area-averaged mean variables evaluated at the tower outlet, being the axial velocity, tangential velocity, and pressure, for each GCI test are compared. It should be mentioned that, in the GCI test, the data are collected in the case with a fixed crosswind velocity of 4 m/s and the swirl source zone located right above the heat exchangers (zone 1) with a prescribed angular frequency of $\omega = 1$ s$^{-1}$. The GCI can be expressed as

$$GCI_{i+1,i} = \frac{Fs}{Rf^N - 1}\left|\frac{f_{i+1} - f_i}{f_i}\right| \quad (7)$$

where $Fs$ has been recommended to be 1.25 when three or more meshes are available [38]; $N$ is expressed as

$$N = \ln\left(\frac{1}{Rc_i}\right) \Big/ \ln(Rf) \tag{8}$$

where $Rc_i$ is written for the $i^{th}$ mesh as

$$Rc_i = \frac{f_i - f_{i-1}}{f_{i+1} - f_i} \tag{9}$$

Note that all the calculated convergence ratio values are between 0 and 1, so a monotonic convergence is guaranteed in each case.

The results are listed in Table 3. As seen, all the GCI values decrease with the refinement of the mesh. The major differences are among the pressure GCI values. The fourth mesh with 2.42 million grids is finally selected in this study since moving from it to a finer one with 1.5 times as many grids leads to the GCI values of the variables to be less than 0.2%.

The mesh selected in the CFD model is shown in Fig. 3, where the thickness of the first cell layer on both sides of the tower wall is 0.8 mm to satisfy $y^+ \approx 1$, and the inflation rate is less than 1.2. The maximum cell size inside the tower is 0.2 m, while finer meshes are used at the interfaces or regions with sharp gradients for instance the porous zone (heat exchangers) and swirl source zones where the cell sizes are less than 0.1 m.

## 3. CFD model validation

Previous relevant experimental investigations were basically on pipe swirls [20,39,40] or free swirls [41,42]. In addition to the different ranges of Reynolds number and Froude number, their source boundary conditions were set values for inlet velocity, which is totally different from our source boundary condition – a heat exchanger (or radiator model). Thus, it might not be acceptable to validate a buoyancy driven flow with a velocity driven one. However, in the absence of swirling effects, validations can be conducted with experimental data in terms of short NDDCTs; i.e. Gatton tower [3], with no windbreak walls installed.

In the Gatton tower experiment, temperature sensors were evenly mounted at four cross-sections, i.e., the top layer (14 m height above the heat exchangers), middle layer (7 m height above the heat exchangers), bottom layer (0.8 m height above the heat exchangers), and inlet layer (0.5 m height below the heat exchangers), respectively; see Fig. 4. In addition, each of the heat exchanger bundles was equipped with two temperature sensors: inlet and outlet. The wind speed and direction were collected by two anemometers nearby the cooling tower at 5 m elevation, which is consistent with the reference height in Eq. (6).

Several time intervals longer than 1000 s, within which the wind speeds are relatively stable in each test, are selected for the temperature validation, as presented in Fig. 5. Since the wind direction changes with time in the experiment, while it is fixed in CFD simulations, the space-averaged data are first adopted to eliminate this deviation. The averaged heat exchanger temperature is calculated based on inlet and outlet temperatures of all the heat exchanger bundles, while the averaged bottom layer temperature is prescribed base on data from 9 evenly mounted sensors shown in Fig. 4. As seen, all the temperature changes within the time intervals are insignificant, indicating that the time-averaged counterparts are reliable.

Then the time-averaged data, including crosswind speed $u_{cw}$, ambient $T_\infty$, heat exchanger $T_{hx}$, and bottom layer temperatures $T_{bl}$, for each case from Fig. 5 are obtained as listed in Table 4, with $E$ and $N$ representing the experimental and numerical results, respectively. As seen, the CFD simulation results show good agreements with the experimental ones, with the maximum error being less than 3%.

**Table 3**
Summary of the GCI calculation for selected variables on different meshes.

| Area-averaged mean variables | $GCI_{21}$ (%) | $GCI_{32}$ (%) | $GCI_{43}$ (%) | $GCI_{54}$ (%) |
|---|---|---|---|---|
| Axial velocity | 9.54 | 3.42 | 0.64 | 0.18 |
| Tangential velocity | 3.39 | 0.74 | 0.27 | 0.1 |
| Pressure | 6.96 | 3.13 | 0.46 | 0.14 |

## 4. Results and discussion

The simulations are carried out at the crosswind velocities ranging from 0 to 16 m/s with an interval of 4 m/s. Influences of three swirl source zone locations, as illustrated in Fig. 1, are investigated. The solid body rotation ($u_\theta = r\omega$) is introduced in the swirl source zone, while the angular frequency $\omega$ varies from 0 to 3 $s^{-1}$ with an interval of 0.5 $s^{-1}$. The convective heat transfer rate $Q_{hx}$ of the radiator is adopted to evaluate the thermal performance of the NDDCT as

$$Q_{hx} = \int_A h_{hx}(T_{hx} - T_{ad})\,dA = \int_A q_{hx}\,dA \tag{10}$$

### 4.1. Windless conditions and cold air inflow penetration

In this subsection, swirling effects are investigated in the absence of crosswind. Fig. 6 shows the transient result of the heat transfer rate through the tower without swirl inputs. The transient process can be divided into three phases: tower start-up process (0~130 s); cold air inflow penetration (130~190 s); quasi-steady state with cold air inflow (after 190 s). Though the heat transfer rate shows a steady solution after $t = 190$ s in this transient result, the flow field, or specifically the location where cold air penetrates into the tower, differs from time to time, as shown in Fig. 7. This is totally different from the streamline pattern in our 2-D simulation results [19], because the previous axisymmetric assumption does not apply in the 3-D ones, and this strong lack of axisymmetric pattern is more practical since the cold air inflow was never found to be axisymmetric in buoyant duct flow experiments, as indicated in [3,43]. Hence, it is rather a quasi-steady state solution in the presence of cold air inflow after 190 s.

When cold air inflow occurs, the air draft velocity through the tower is significantly reduced, and so is the heat transfer rate. A pioneering experimental study on buoyant flows in open-topped vessels, has pointed out that the cold air penetration depth is inversely proportional to the aspect ratio, Froude number and Reynolds number, for cases with turbulent boundary layers on a smooth wall. Since the short NDDCT adopted in this study features with a low draft capacity and a high heat exchangers resistance, resulting in an extremely low Froude number and thus provokes cold air inflow penetration. Our previous studies have indicated that inducing swirls inside the tower is able to reduce this unfavourable effect by means of thinning the boundary layer thickness [6] and expand the contraction effect of the so-called lazy plume [19]. Hence, swirling motions ($\omega = 0.5\ s^{-1}$) are introduced at different locations inside the tower after the cold air inflow penetration ($t = 500$ s), and the transient results are present in Fig. 8. As seen, the heat transfer rate reduced by cold air inflow can be recovered after inducing swirling motions, but the transient characteristic varies from each other. Stable states (steady or periodic state) can be reached whatever location the swirl is introduced. Further, it takes the longest time to reach the stable (steady) state with the swirl induced right above the heat exchangers (zone 1), but it shows the highest thermal performance among the three cases. Periodic patterns are found in cases with swirl input by zone 2 and 3, and the latter holds the lowest time-averaged mean thermal performance. In the two cases, the cold air inflow effects are reduced but not eliminated as that in the case with swirl zone 1. After the cold air intrudes, the hot air velocity through the tower decreases, resulting in an increase in the air temperature of the main flow due to the fixed heat exchanger temperature. This increased main flow temperature also enhances the buoyancy effect, which is able to push back against the cold air inflow, especially when it is reduced by swirling motions. Once it happens, the average air draft velocity, in turn, increases while the temperature decreases, and when it is not capable of pushing the cold air

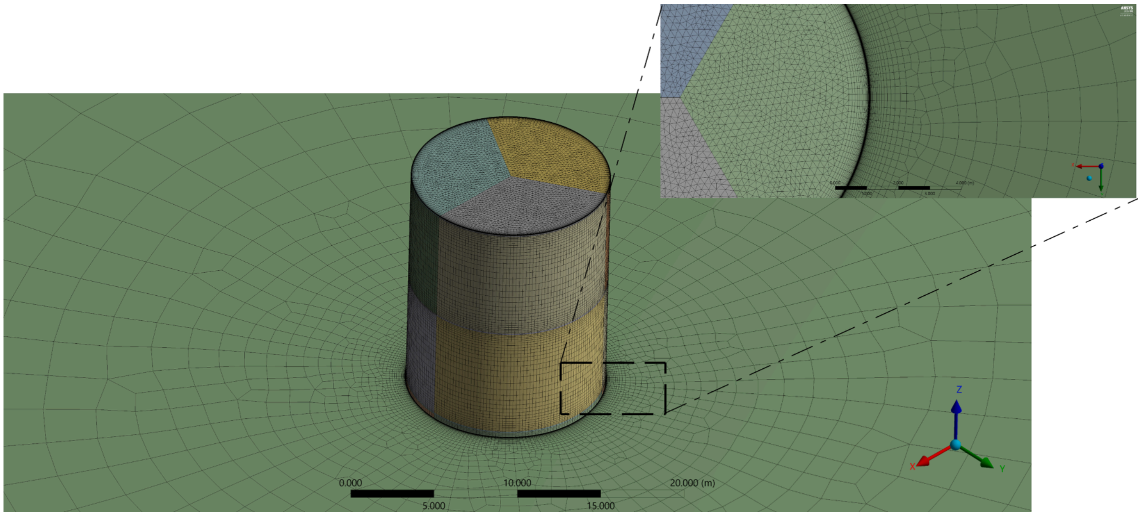


**Fig. 3.** Refined meshes inside and outside of the cooling tower.

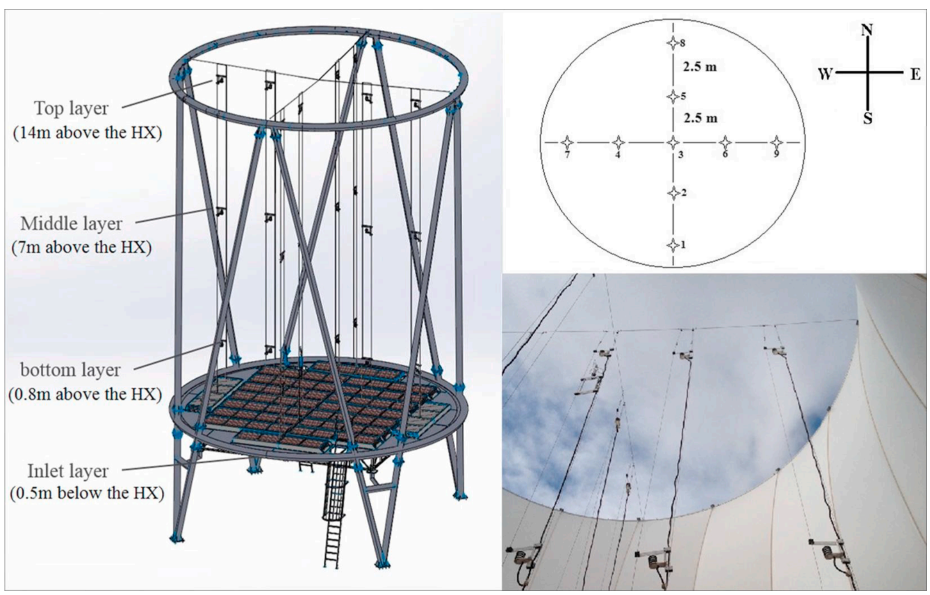


**Fig. 4.** Test sensors distribution in Gatton tower.

inflow upwards, the cold air intrudes back again and thus leads to the periodic patterns.

The velocity streamlines in the presence of swirls at $t = 1000$ s are demonstrated in Fig. 9. As observed, the cold air inflow disappears in the case with swirl zone 1, while it can be obviously found in the case with swirl zone 3. This is due to the solid body rotation induced in the source zone, and consequently the highest local pressure occurs close to the wall while the lowest counterpart is at the centreline. As a result, a sudden pressure change along the axial direction near the wall between the downstream and the source zone happens. Meanwhile, the cold air inflow penetrates from the tower outlet near the wall, and when the source zone is mounted there, the sudden pressure change increases the resistance from pushing the cold air inflow upwards.

By continuously increasing the swirl intensity for all cases at the windless condition, it is found steady states can be finally reached. Along with the time-averaged mean heat transfer rate results in Figs. 6 and 8, the general thermal performance can be yielded in Fig. 10. With the tangential velocity increasing, the heat transfer rate enhanced by swirl inputs located at the tower outlet (zone 3) gradually exceeds the counterparts in cases with swirl zone 1 and 2. The mechanism is illustrated with the aid of pressure contours presented in Fig. 11. Our previous study [19] has proven that swirling motions cannot influence the cross-section area-weighted averaged mean axial pressure gradient inside the tower. However, swirl can lower the gauge pressure at the tower outlet, which in turn decreases the gauge pressure at the heat exchangers elevation, leading to a higher draft speed. The effect increases with the swirl intensity, which agrees with observations presented in Fig. 11. In addition, when swirl is introduced inside the tower, which is analogous to the swirl inside pipes as reported in [20–22], the swirl intensity decays due to the boundary layer influence and turbulence dissipation. Hence, focusing on reducing the cold air inflow effects, introducing swirling motions right above the heat exchangers is found to be the optimal location for recovering the thermal performance by around 40% with angular frequency input of 1 $s^{-1}$, while swirl located at the tower outlet performs the best on the air draft speed enhancement, and thus further increases approximately 17% of the heat transfer rate with angular frequency input of 2 $s^{-1}$, after cold air inflow is eliminated.

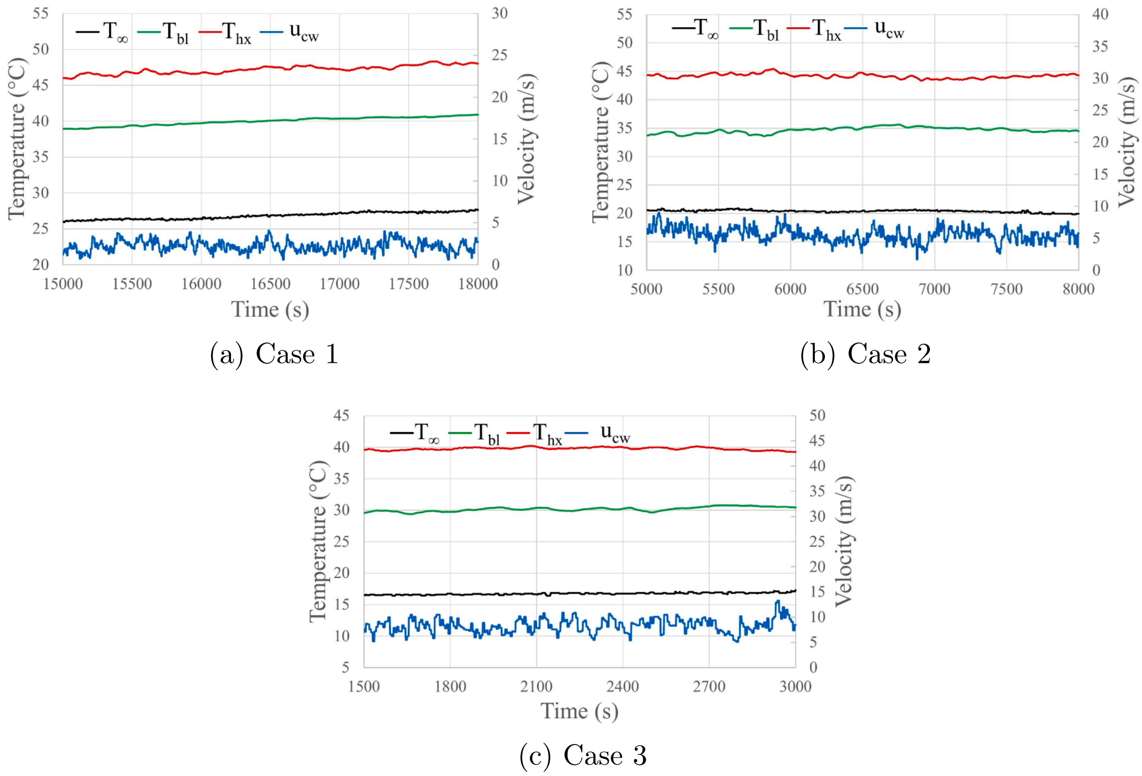


**Fig. 5.** Data collected from the Gatton tower experiment at different conditions corresponding to the cases in Table 4.

**Table 4**
Comparison between experimental and numerical results.

| Case | $u_{cw}$ (m/s) | $T_\infty$ (°C) | $T_{hx}$ (°C) | $T_{bl}$ (°C)($E\|N$) | Error |
|---|---|---|---|---|---|
| 1 | 2.23 | 26.82 | 47.19 | 39.99\|40.56 | 1.4% |
| 2 | 5.56 | 20.39 | 44.17 | 34.65\|35.09 | 1.3% |
| 3 | 8.34 | 16.74 | 39.77 | 30.18\|30.97 | 2.6% |

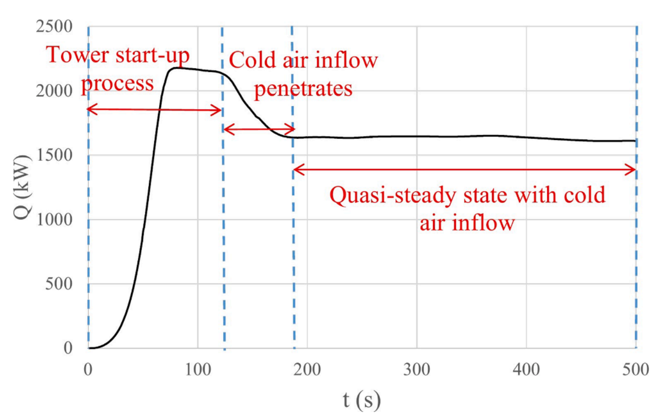


**Fig. 6.** Transient result of heat transfer rate through the tower ($u_{cw} = 0$ m/s; $\omega = 0\,s^{-1}$).

### 4.2. Swirl effects on windy conditions

In this subsection, swirling effects are investigated in the presence of crosswind, with the tri-blade-like windbreak walls. In Fig. 12, the heat transfer rate from the tower is plotted against the angular frequency of the input swirl at the crosswind speeds of $4, 8, 12, 16$ m/s. Apparently, the thermal performance of the tower improves with the swirl angular frequency. Among the three swirl input locations, cases of zone 3 consistently show the best enhancement when $\omega$ exceeds $1\,s^{-1}$, and larger the tangential velocity input, the more significant the superiority. Cross-overs are observed when $\omega$ varies from 0 to $0.5\,s^{-1}$. Cases of zone 2 are observed to be inferior to the other two locations when $\omega$ is over $0.5\,s^{-1}$. With the same high angular frequency, i.e. $\omega = 2\,s^{-1}$, the increment on the heat transfer rate is around 17% at the wind speed of 4 m/s, while it is approximately 11% at that of 16 m/s. The three lines under all the wind speeds generally illustrate that the thermal performance enhancement, or its increasing gradient, increases first and then decreases.

Fig. 13 presents the velocity streamlines passing through the tower at the crosswind speed of 4 m/s and 8 m/s with different swirl angular frequencies when the swirl zone is located right above the heat exchangers (swirl zone 1). As seen, the cold air inflow penetration disappears in comparison with Fig. 9, which explains that, in the absence of swirl ($\omega = 0\,s^{-1}$), the thermal performance in Fig. 12 (a) is by far better than those reported in Fig. 10. It has also been reported that the cold air inflow becomes negligible when crosswind speed is over 2 m/s in Gatton tower [33]. As discussed in [19], a contraction effect occurs on the plume released from the tower outlet as a result of significantly low *Fr*, which provokes more cold air mixing with hot air right above the tower outlet near the edge, further boosting the cold air penetration. As crosswind speed increases, the plume leaving the tower bends further leeward, and consequently the cold air inflow penetration disappears with the contraction effect. Additionally, to quantify the uniformity of the axial velocity inside the tower, the tower body is divided into 15 cross-sections uniformly with the interval of 1 m. Then the area-weighted uniformity index $\gamma$, in terms of axial velocity, is calculated on each cross-section, so that the volume-averaged uniformity index $\overline{\gamma}$ can be estimated as

$$\overline{\gamma} = \frac{1}{15}\Sigma_{j=1}^{15}\gamma_j \tag{11}$$

where

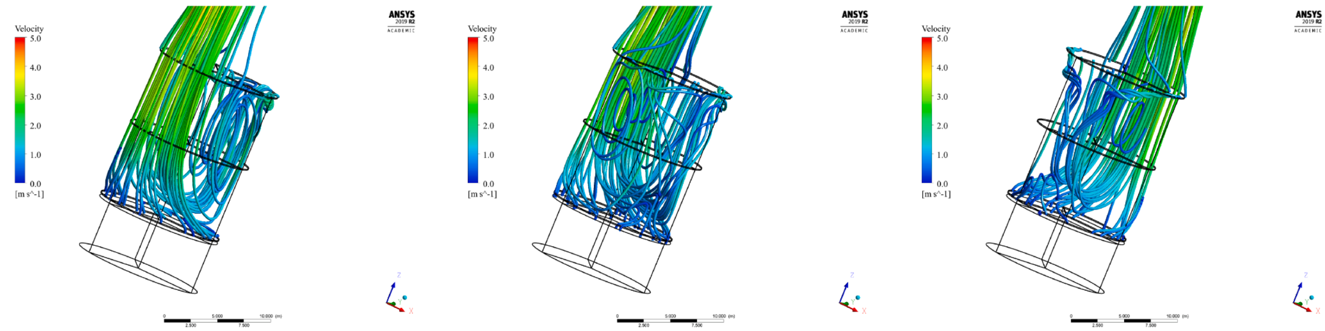

(a) $t = 190\ s$ (b) $t = 300\ s$ (c) $t = 400\ s$

**Fig. 7.** Velocity streamlines at the quasi-steady state with cold air inflow penetration at different times ($u_{cw} = 0$ m/s; $\omega = 0$ s$^{-1}$).

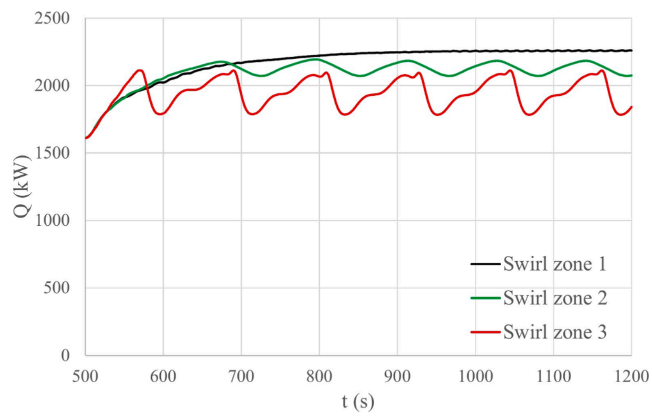


**Fig. 8.** Transient result of heat transfer rate with different swirl input locations after cold air inflow penetration ($u_{cw} = 0$ m/s; $\omega = 0.5$ s$^{-1}$).

$$\gamma = 1 - \frac{\Sigma_{i=1}^{n}\left[\left(\left|X_i - \overline{X}\right)A_i\right]}{2\overline{X}\Sigma_{i=1}^{n}A_i} \tag{12}$$

and $i$ is the facet index of the surface with $n$ facets; $\overline{X}$ is the area-weighted mean averaged variable over the surface; $j$ represents the cross-sections. As observed in Fig. 13, the velocity streamlines inside the tower with swirls are more uniform than that without swirl. This is anticipated as the crosswind passing underneath the heat exchangers is guided by the tri-blade-like windbreak walls towards the heat exchanger, and specifically the crosswind is guided upward in the windward section while separations of the air flow is provoked at the tips of windbreak walls in the leeward sections. Besides, the crosswind speed is higher at the tower outlet elevation than that of the heat exchangers elevation due to the velocity profile, which causes the streamlines slightly bending leewards even before leaving the tower; see Fig. 13. However, with the swirl momentum introduced, the bending streamlines inside the tower are influenced by the rotating motion, and thus the axial velocity field becomes more uniform.

As a result of non-uniform axial velocity inside the tower, the heat transfers through the heat exchangers non-uniformly as well. This is clearly observed in Fig. 14, which illustrates the heat flux contours on the upper surface of the heat exchangers. As seen, the majority of heat is exchanged in the windward section. As mentioned before, the crosswind is guided upward in the windward section by the windbreak walls, so the upward air velocity there contains both guided crosswind and buoyant draft. With the increment of tangential velocity input in swirl zone 1, not

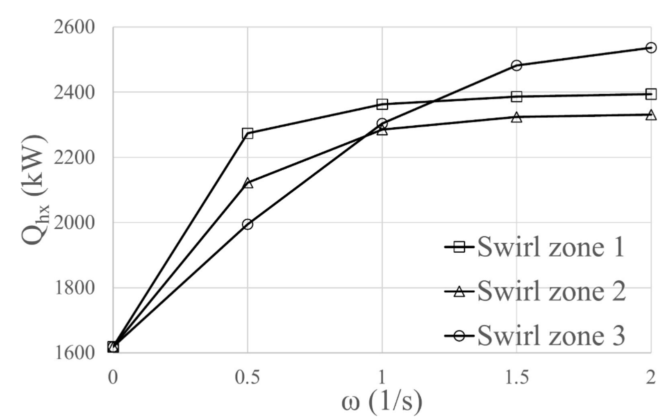


**Fig. 10.** Heat transfer rate versus tangential velocity intensity with different swirl input locations at no wind condition.

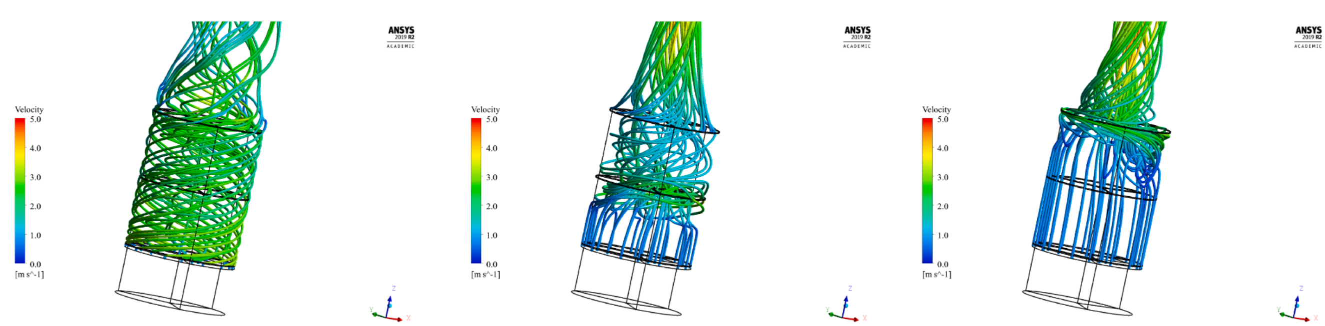

(a) Swirl zone 1 (b) Swirl zone 2 (c) Swirl zone 3

**Fig. 9.** Velocity streamlines with different swirl input locations at $t = 1000$ s ($u_{cw} = 0$ m/s; $\omega = 0.5$ s$^{-1}$).

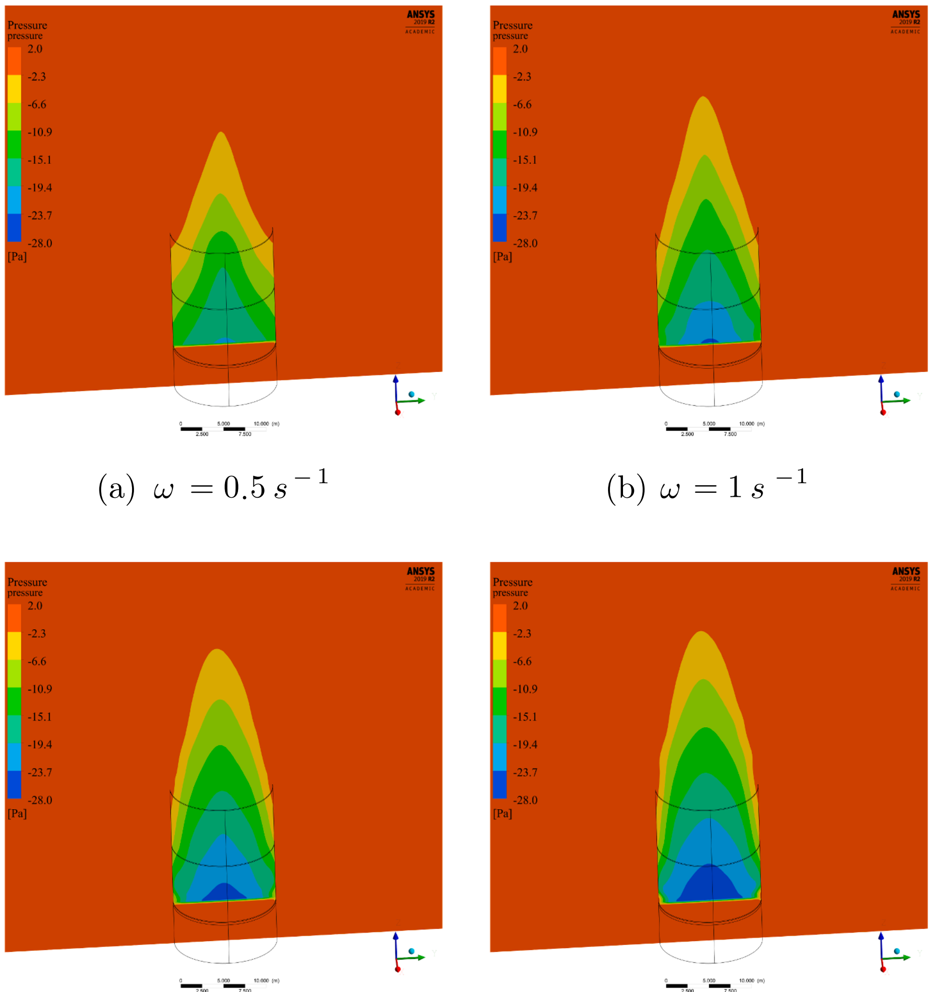


(a) $\omega = 0.5\,s^{-1}$ (b) $\omega = 1\,s^{-1}$ (c) $\omega = 1.5\,s^{-1}$ (d) $\omega = 2\,s^{-1}$

**Fig. 11.** Pressure contours with swirl input at no wind condition (swirl zone 1).

only the heat flux becomes more uniform, but also the overall heat transfer rate increases. The upward air inside the tower is spun by the input tangential momentum, leading to a more uniform flow field, i.e. axial velocity and temperature, so does the heat flux. Similar to cases in the absence of crosswind, the overall heat transfer rate enhanced by swirl is explained by the lower gauge pressure at the tower outlet elevation caused by tangential momentum. Consequently the pressure at heat exchangers elevation is reduced and the air draft speed is increased.

Fig. 15 shows the gauge pressure and area-averaged mean tangential velocity at the tower outlet with three swirl input locations at $u_{cw} = 16$ m/s. Among the three locations, the tangential velocity with swirl zone 3 presents the highest intensity due to the 0 decay rate while that with swirl zone 2 corresponds to a minimum value, and consequently the gauge pressures demonstrate the contrary trend; see [19]. This is interesting since, intuitively, the decay distance of swirl zone 2 is shorter than that of swirl zone 1.

To understand that, corresponding velocity vectors and streamlines are presented in Figs. 16 and 17. As seen in Fig. 16, obvious circulation zones are found adjacent to the wall in the case of swirl input at the middle layer of the tower (zone 2), while they are found to be much smaller in the cases with swirl input right above the heat exchangers (zone 1) and tower outlet (zone 3). This is because the tangential velocity we introduced is the solid body rotation, leading to the largest tangential velocity value occurring near the wall, where the highest pressure is consequently observed along the radial direction. When the swirl source zone is mounted at the tower middle layer, this radial pressure profile will cause a sudden pressure change in the axial direction near the wall. Specifically, the axial velocity near the wall is usually very low due to the boundary layer effect, and once the dynamic pressure there is not large enough against the sudden pressure change, a back flow forms leading to the circulation zones. This prevents the swirl effects from unrestrictedly enhancing the thermal performance of the tower, and thus it is found that the increasing gradient on the heat rejection rate gradually reduces when $\omega$ exceeds 1 $s^{-1}$ for each case in Fig. 12. However, when the swirl generator is located right above the heat exchanger, the back flows are unlikely to be created because of the high resistance of the porous media upstream, while circulations in the case of swirl input at the tower outlet are highly affected by the crosswind. Hence, when swirl is generated at source zone 2, the axial change of tangential momentum is influenced by the highest circulations and thus part of the high magnitude swirl flows downwards then upwards. Consequently, the swirl intensity of this part of tangential momentum decays below source zone 2, and the higher the angular frequency input, the larger the swirl intensity decays, pertinent to the velocity streamlines of cases with swirl zone 2 in Fig. 17, at which the highest magnitude of velocity inside the tower is below the tower middle layer. This explains why the heat transfer rate in cases of swirl zone 2 holds the lowest performance with higher swirl intensities in Fig. 12.

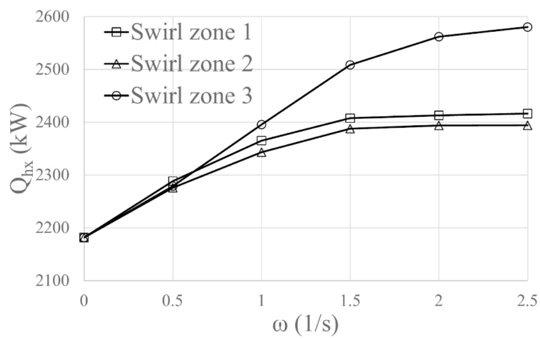


(a) $u_{\mathrm{cw}} = 4\,m/s$

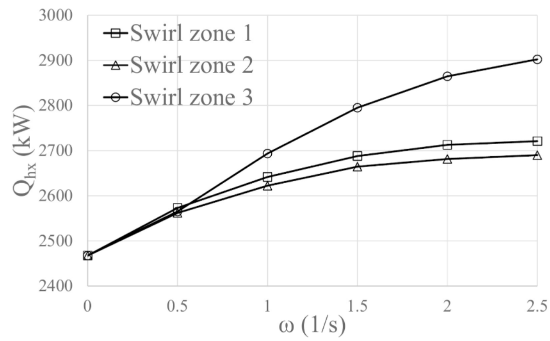


(b) $u_{\mathrm{cw}} = 8\,m/s$

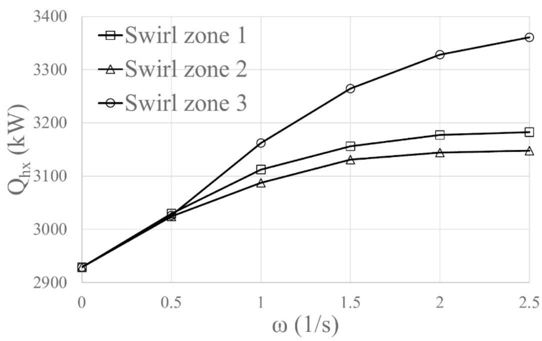


(c) $u_{\mathrm{cw}} = 12\,m/s$

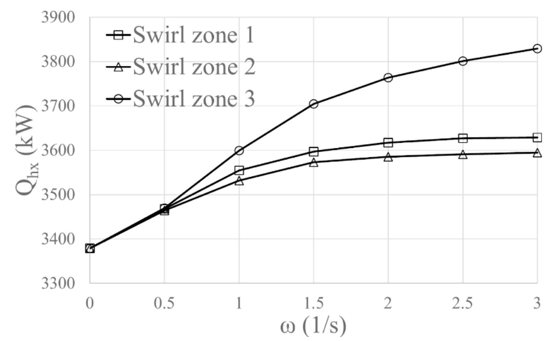


(d) $u_{\mathrm{cw}} = 16\,m/s$

**Fig. 12.** Heat transfer rate versus tangential velocity intensity with different swirl input locations at different crosswind speeds.

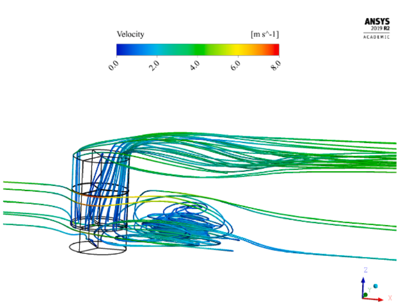

(a) $u_{\mathrm{cw}} = 4\,m/s$, $\omega = 0\,s^{-1}$, $\overline{\gamma}(u_z) = 0.731$

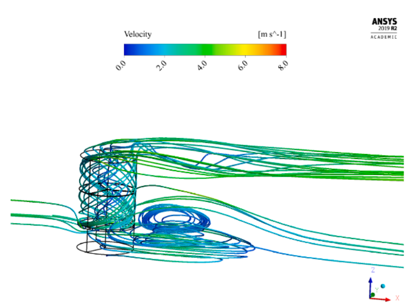

(b) $u_{\mathrm{cw}} = 4\,m/s$, $\omega = 0.5\,s^{-1}$, $\overline{\gamma}(u_z) = 0.816$

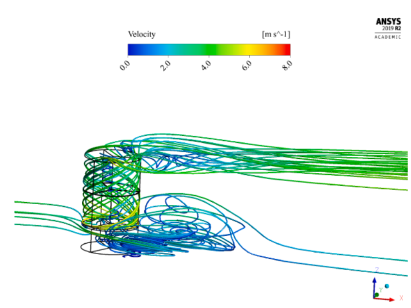

(c) $u_{\mathrm{cw}} = 4\,m/s$, $\omega = 1\,s^{-1}$, $\overline{\gamma}(u_z) = 0.823$

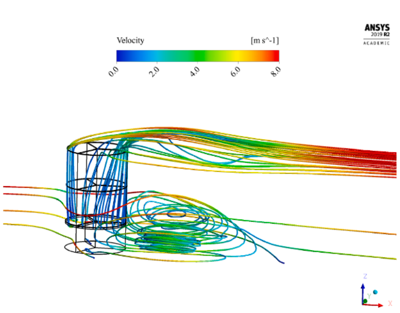

(d) $u_{\mathrm{cw}} = 8\,m/s$, $\omega = 0\,s^{-1}$, $\overline{\gamma}(u_z) = 0.694$

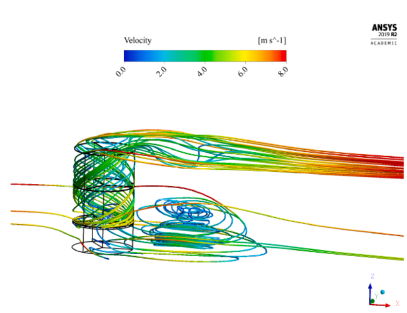

(e) $u_{\mathrm{cw}} = 8\,m/s$, $\omega = 1\,s^{-1}$, $\overline{\gamma}(u_z) = 0.729$

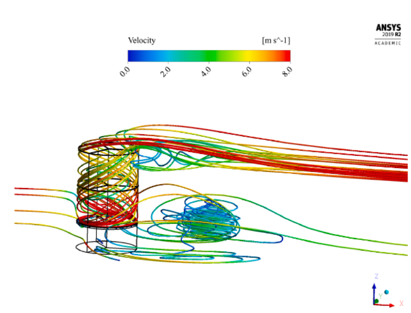

(f) $u_{\mathrm{cw}} = 8\,m/s$, $\omega = 2\,s^{-1}$, $\overline{\gamma}(u_z) = 0.736$

**Fig. 13.** Side views of velocity streamlines passing through the tower with swirl input right above the heat exchangers (Swirl zone 1).

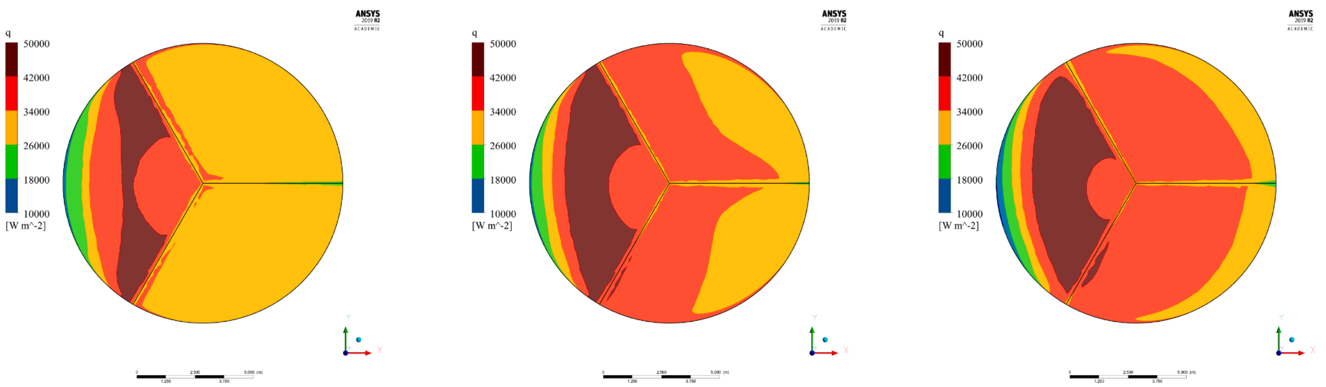

(a) $u_{\mathrm{cw}} = 4\ m/s, \omega = 0 s^{-1}, \gamma(q) = 0.877$  (b) $u_{\mathrm{cw}} = 4\,m/s,\ \omega = 0.5\,s^{-1},\ \gamma(q) = 0.903$  (c) $u_{\mathrm{cw}} = 4\,m/s,\ \omega = 1\,s^{-1},\ \gamma(q) = 0.918$

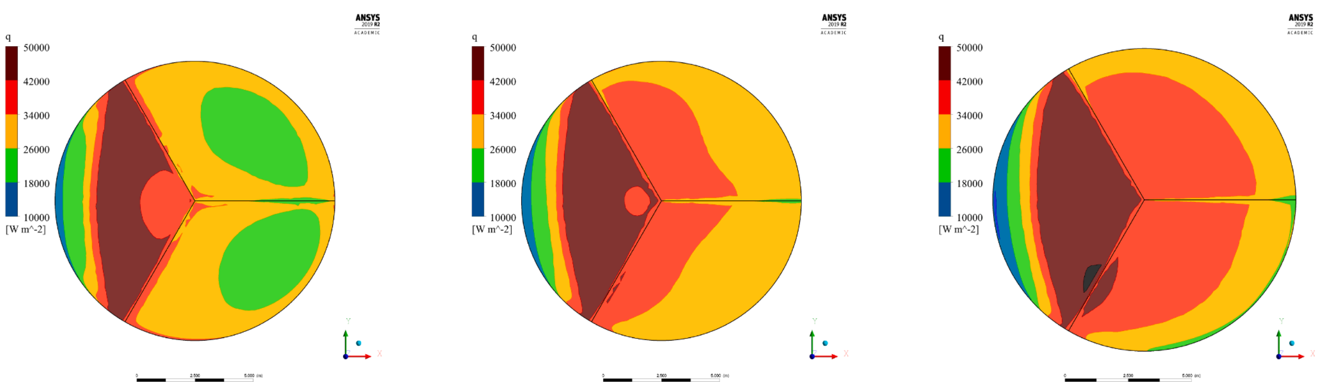

(d) $u_{\mathrm{cw}} = 8\,m/s,\ \omega = 0\,s^{-1},\ \gamma(q) = 0.783$  (e) $u_{\mathrm{cw}} = 8\,m/s,\ \omega = 1\,s^{-1},\ \gamma(q) = 0.806$  (f) $u_{\mathrm{cw}} = 8\,m/s,\ \omega = 2\,s^{-1},\ \gamma(q) = 0.831$

**Fig. 14.** Heat flux contours at the upper surface of heat exchangers with swirl input right above the heat exchangers (Swirl zone 1).

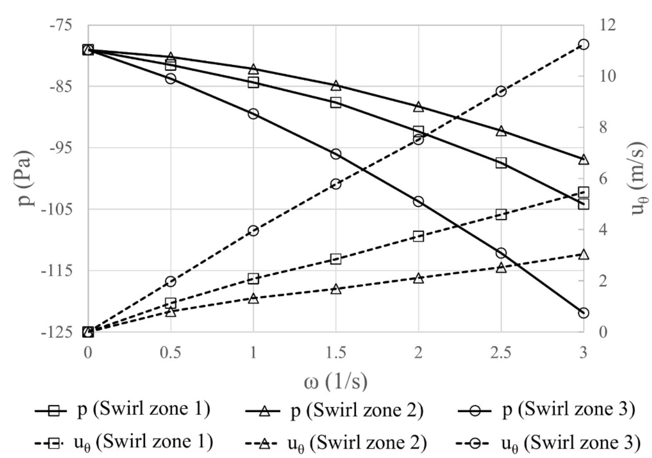


**Fig. 15.** Gauge pressure and area-averaged mean tangential velocity at the tower outlet at $u_{\mathrm{cw}} = 16$ m/s.

### 4.3. Energy efficiency analysis

To analyse the energy efficiency, the energy consumed and gained by swirl inputs needs to be compared. First, the rotation energy consumption can be estimated by the product of volume flow rate and total pressure change. Though the local static pressure changes depending on the tangential velocity profile, the cross-section area-weighted mean averaged static pressure difference between the upstream and downstream of the swirl source zone is negligible, as reported in [19]. Hence, the consumed energy can be approximated, with the swirl generator efficiency $\eta_\phi$, by

$$Q_\phi = \frac{\frac{1}{2}\rho r^2 \omega^2 \int_A u_z \,\mathrm{d}A}{\eta_\phi} \tag{13}$$

From engineering purposes, a cost-effectiveness analysis requires the comparison between this power consumption and the power outcome difference caused by swirl. However, the power outcome depends on the type of power cycle, system components, efficiency of each component, and each input parameter. Thus, the swirl enhanced thermal performance of the tower is compared with the energy requirement for generating the swirling motions. Given that the swirl located at the tower outlet generally shows a superiority on the thermal performance to other locations on windy conditions, source zone 3 is selected. By assuming the source generator efficiency as $\eta_\phi = 80\%$, the comparison is illustrated in Fig. 18, at which the solid lines represent the heat rejection rate improvement while the dash lines stand for the energy consumptions. As expected, increasing the tangential velocity results in the increments in both of them. However, the slopes of the increments are completely opposite. The decreasing trend in the heat rejection rate enhancement is due to the side effects caused by excessively strong swirl as mentioned before, while the increasing trend in the energy

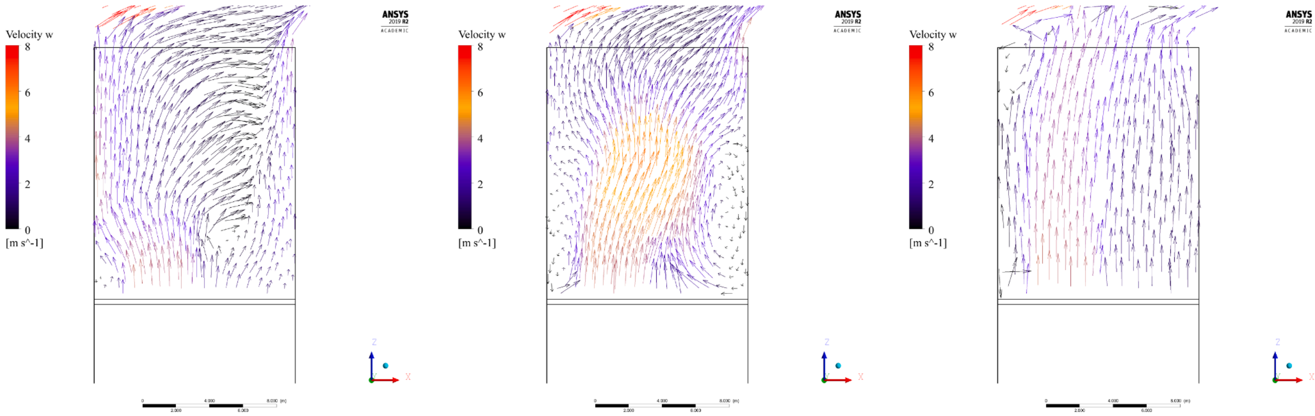


(a) Swirl zone 1 (b) Swirl zone 2 (c) Swirl zone 3

**Fig. 16.** Velocity vectors at x-z plane ($u_{cw} = 16$ m/s, $\omega = 2$ s$^{-1}$).

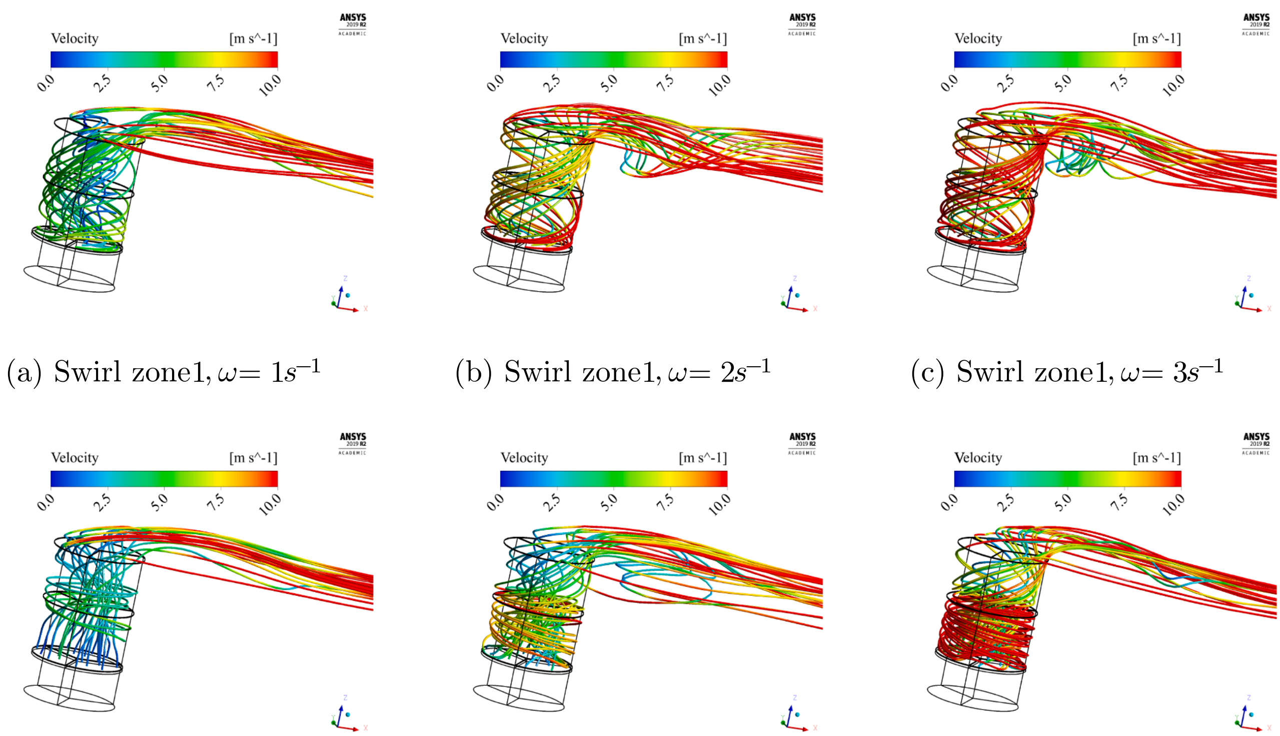


(a) Swirl zone1, $\omega = 1s^{-1}$ (b) Swirl zone1, $\omega = 2s^{-1}$ (c) Swirl zone1, $\omega = 3s^{-1}$

(d) Swirl zone2, $\omega = 1s^{-1}$ (e) Swirl zone2, $\omega = 2s^{-1}$ (f) Swirl zone2, $\omega = 3s^{-1}$

**Fig. 17.** Velocity streamlines at $u_{cw} = 16$ m/s.

consumption is led by the square of $\omega$ in Eq. (13). This further proves that one cannot unlimitedly improve the thermal performance of the tower by continuously increasing the tangential momentum. In addition, the heat transfer rate improvements generally show an overlap at different crosswind speeds. In contrast, with the aid of the windbreak walls, the air draft velocity increases with the crosswind speed, which further increases the energy consumption in accordance with Eq. (13). Within the range of the tangential momentum inputs in this study, the largest energy consumption is around 40 kW, while the corresponding heat rejection rate improvement caused by the swirl is over 400 kW. Though it could be inappropriate to compare heat transfer rate with power, it still provides a qualitative analysis on the feasibility of swirl enhanced NDDCTs.

## 5. Conclusions

3-D simulations have been carried out to investigate the swirl effects on the thermal performance of a short natural draft dry cooling tower both in the absence and presence of crosswind. The tri-blade-like windbreak walls with the optimized angle of attack 0° have been installed underneath the heat exchangers to mitigate the crosswind effect. Swirls have been generated by mounting tangential momentum source zones with solid body rotations inside the tower at three different elevations: right above the heat exchangers (zone 1); middle layer of the tower (zone 2); tower outlet (zone 3). The main findings are listed as following:

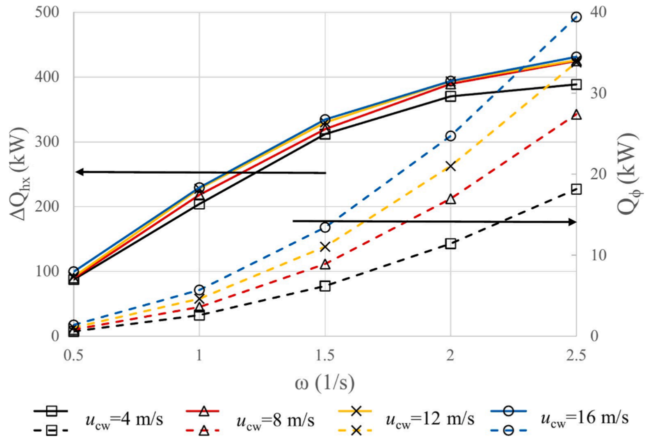


**Fig. 18.** Comparison between the heat rejection rate improvement and energy consumption caused by swirls (swirl zone 3).

- On windless conditions, introducing swirling motions right above the heat exchangers, at the angular frequency input of 0.5 $s^{-1}$, is found to be the optimal location for improving around 40% of the reduced thermal performance, which is caused by the cold air inflow penetration. As the swirl intensity further increases, the cold air inflow can be eliminated whichever location the swirl is generated. Additionally, locating tangential momentums at the tower outlet instead performs the best on the air draft speed enhancement after the cold air inflow is eliminated, and thus further increases approximately 17% of the heat transfer rate at the angular frequency input of 2 $s^{-1}$.
- In the presence of crosswind and windbreak walls, air flows through the heat exchangers and tower non-uniformly. By mounting the swirl generator right above the heat exchangers, the uniform index of the heat flux can be improved by 5% with 1 $s^{-1}$ angular frequency input. More importantly, inducing swirls at the tower outlet is still the optimal choice for increasing the air draft speed through the tower. Depending on the crosswind speed, the heat rejection rate of the tower can be enhanced by 11~17% at the angular frequency input of 2 $s^{-1}$.
- The energy efficiency analysis indicates that, within the range of the tangential momentum inputs in this study, the largest energy consumption is around 40 kW, while the corresponding heat rejection rate improvement caused by the swirl is over 400 kW.

## Declaration of Competing Interest

The authors declare that they have no known competing financial interests or personal relationships that could have appeared to influence the work reported in this paper.

## Acknowledgements

This research was performed as part of the ARC DECRA (Discovery Early Career Research Award) project DE190101253. The authors would like to thank Australian Solar Thermal Research Institute (ASTRI) and China Scholarship Council (CSC) for their financial support.

## References

[1] Australia's off-grid clean energy market research paper, AECOM, Canberra, 2014.
[2] Y. Lu, Small natural draft dry cooling towers for renewable power plants, Ph.D. thesis, The University of Queensland, 2015.
[3] X. Li, Numerical and experimental study of small natural draft dry cooling tower for concentrating solar thermal power plant, Ph.D. thesis, The University of Queensland, 2018.
[4] G. Hunt, N. Kaye, Lazy plumes, J. Fluid Mech. 533 (2005) 329–338.
[5] P. Dong, X. Li, Y. Sun, K. Hooman, Z. Guan, Y. Dai, H. Gurgenci, Numerical investigation of the influence of local effects on the transient start-up process of natural draft dry cooling towers in dispatchable power plants, Int. J. Heat Mass Transf. 133 (2019) 166–178.
[6] Y. Dai, A.S. Kaiser, Y. Lu, A.Y. Klimenko, P. Dong, K. Hooman, Addressing the adverse cold air inflow effects for a short natural draft dry cooling tower through swirl generation, Int. J. Heat Mass Transf. 145 (2019) 118738.
[7] A. Du Preez, D. Kröger, Effect of wind on performance of a dry-cooling tower, Heat Recovery Syst. CHP 13 (2) (1993) 139–146.
[8] K. Hooman, Theoretical prediction with numerical and experimental verification to predict crosswind effects on the performance of cooling towers, Heat Transfer Eng. 36 (5) (2015) 480–487.
[9] A. Du Preez, D. Kröger, The effect of the heat exchanger arrangement and wind-break walls on the performance of natural draft dry-cooling towers subjected to cross-winds, J. Wind Eng. Ind. Aerodyn. 58 (3) (1995) 293–303.
[10] Z. Zhai, S. Fu, Improving cooling efficiency of dry-cooling towers under cross-wind conditions by using wind-break methods, Appl. Therm. Eng. 26 (10) (2006) 1008–1017.
[11] M. Goodarzi, R. Keimanesh, Heat rejection enhancement in natural draft cooling tower using radiator-type windbreakers, Energy Convers. Manage. 71 (2013) 120–125.
[12] L. Chen, L. Yang, X. Du, Y. Yang, Performance improvement of natural draft dry cooling system by interior and exterior windbreaker configurations, Int. J. Heat Mass Transf. 96 (2016) 42–63.
[13] W. Wang, L. Chen, X. Huang, L. Yang, X. Du, Performance recovery of natural draft dry cooling systems by combined air leading strategies, Energies 10 (12) (2017) 2166.
[14] T. Wu, Z. Ge, L. Yang, X. Du, Flow deflectors to release the negative defect of natural wind on large scale dry cooling tower, Int. J. Heat Mass Transf. 128 (2019) 248–269.
[15] H. Ma, F. Si, Y. Kong, K. Zhu, W. Yan, Wind-break walls with optimized setting angles for natural draft dry cooling tower with vertical radiators, Appl. Therm. Eng. 112 (2017) 326–339.
[16] H. Ma, F. Si, K. Zhu, J. Wang, The adoption of windbreak wall partially rotating to improve thermo-flow performance of natural draft dry cooling tower under crosswind, Int. J. Therm. Sci. 134 (2018) 66–88.
[17] H. Ma, F. Si, J. Wang, Study on the effects of apex angle of the delta-type radiator on thermo-flow performance of natural draft dry cooling tower, Int. J. Heat Mass Transf. 148 (2020) 119002.
[18] Y. Lu, A. Klimenko, H. Russell, Y. Dai, J. Warner, K. Hooman, A conceptual study on air jet-induced swirling plume for performance improvement of natural draft cooling towers, Appl. Energy 217 (2018) 496–508.
[19] Y. Dai, Y. Lu, A.Y. Klimenko, Y. Wang, K. Hooman, Theoretical and numerical investigations of swirl enhanced short natural draft dry cooling towers, Appl. Therm. Eng. (2020) 115783.
[20] F. Kreith, O. Sonju, The decay of a turbulent swirl in a pipe, J. Fluid Mech. 22 (2) (1965) 257–271.
[21] A. Najafi, M. Saidi, M. Sadeghipour, M. Souhar, Numerical analysis of turbulent swirling decay pipe flow, Int. Commun. Heat Mass Transfer 32 (5) (2005) 627–638.
[22] A. Najafi, S. Mousavian, K. Amini, Numerical investigations on swirl intensity decay rate for turbulent swirling flow in a fixed pipe, Int. J. Mech. Sci. 53 (10) (2011) 801–811.
[23] A. Najafi, M. Saidi, M. Sadeghipour, M. Souhar, Boundary layer solution for the turbulent swirling decay flow through a fixed pipe: Sbr at the inlet, Int. J. Eng. Sci. 43 (1–2) (2005) 107–120.
[24] R. Maddahian, A. Kebriaee, B. Farhanieh, B. Firoozabadi, Analytical investigation of boundary layer growth and swirl intensity decay rate in a pipe, Arch. Appl. Mech. 81 (4) (2011) 489–501.
[25] J. Pereira, J. Sousa, Confined vortex breakdown generated by a rotating cone, J. Fluid Mech. 385 (1999) 287–323.
[26] J. Lopez, Axisymmetric vortex breakdown part 1. confined swirling flow, J. Fluid Mech. 221 (1990) 533–552.
[27] C.R. Church, J.T. Snow, J. Dessens, Intense atmospheric vortices associated with a 1000 mw fire, Bull. Am. Meteorol. Soc. 61 (7) (1980) 682–694.
[28] P. Cunningham, S.L. Goodrick, M.Y. Hussaini, R.R. Linn, Coherent vortical structures in numerical simulations of buoyant plumes from wildland fires, Int. J. Wildland Fire 14 (1) (2005) 61–75.
[29] T.-H. Shih, W.W. Liou, A. Shabbir, Z. Yang, J. Zhu, A new k-$\epsilon$ eddy viscosity model for high reynolds number turbulent flows, Comput. Fluids 24 (3) (1995) 227–238.
[30] R. Al-Waked, M. Behnia, The performance of natural draft dry cooling towers under crosswind: Cfd study, Int. J. Energy Res. 28 (2) (2004) 147–161.
[31] A. Escue, J. Cui, Comparison of turbulence models in simulating swirling pipe flows, Appl. Math. Model. 34 (10) (2010) 2840–2849.
[32] G. Gerolymos, I. Vallet, Implicit computation of three-dimensional compressible navier-stokes equations using k-epsilon closure, AIAA journal 34 (7) (1996) 1321–1330.
[33] P. Dong, X. Li, K. Hooman, Y. Sun, J. Li, Z. Guan, H. Gurgenci, The crosswind effects on the start-up process of natural draft dry cooling towers in dispatchable power plants, Int. J. Heat Mass Transf. 135 (2019) 950–961.
[34] K. Hooman, Dry cooling towers as condensers for geothermal power plants, Int. Commun. Heat Mass Transfer 37 (9) (2010) 1215–1220.
[35] FLUENT User's Guide, ANSYS. Inc., USA, 2009.
[36] Y. Zhao, F. Sun, Y. Li, G. Long, Z. Yang, Numerical study on the cooling performance of natural draft dry cooling tower with vertical delta radiators under constant heat load, Appl. Energy 149 (2015) 225–237.
[37] P. Dong, X. Li, A novel method integrating windbreak walls with water distribution to mitigate the crosswind effects on natural draft dry cooling towers, J. Wind Eng. Ind. Aerodyn. 205 (2020) 104318.

[38] P.J. Roache, Quantification of uncertainty in computational fluid dynamics, Ann. Rev. Fluid Mech. 29 (1) (1997) 123–160.
[39] A. Fejer, Z. Lavan, L. Wolf Jr, Measurements of the decay of swirl in turbulent flow, AIAA J. 7 (5) (1969) 971–973.
[40] A. Algifri, R. Bhardwaj, Y. Rao, Eddy viscosity in decaying swirl flow in a pipe, Appl. Sci. Res. 45 (4) (1988) 287–302.
[41] S.-L. Lee, Axisymmetrical turbulent swirling natural-convection plume: Part 2—experimental investigation, J. Appl. Mech. 33 (3) (1966) 656–661.
[42] F. Gallaire, J.-M. Chomaz, Mode selection in swirling jet experiments: a linear stability analysis, J. Fluid Mech. 494 (2003) 223–253.
[43] O. Jörg, R. Scorer, An experimental study of cold inflow into chimneys, Atmospheric Environ. (1967) 1 (6) (1967) 645–654.